

# Dissecting unsupervised learning through hidden Markov modelling in electrophysiological data

Laura Masaracchia<sup>1</sup>, Felipe Fredes<sup>2</sup>, Mark Woolrich<sup>3</sup>, and Diego Vidaurre<sup>1</sup>

<sup>1</sup>Aarhus University Center of Functionally Integrative Neuroscience

<sup>2</sup>Aarhus University

<sup>3</sup>Oxford Centre for Human Brain Activity, Oxford University

January 26, 2023

## Abstract

Unsupervised, data-driven methods are commonly used in neuroscience to automatically decompose data into interpretable patterns. These patterns differ from one another depending on the assumptions of the models. How these assumptions affect specific data decompositions in practice, however, is often unclear, which hinders model applicability and interpretability. For instance, the hidden Markov model (HMM) automatically detects characteristic, recurring activity patterns (so-called states) from time series data. States are defined by a certain probability distribution, whose state-specific parameters are estimated from the data. But what specific features, from all of those that the data contain, do the states capture? That depends on the choice of probability distribution and on other model hyperparameters. Using both synthetic and real data, we aim at better characterising the behaviour of two HMM types that can be applied to electrophysiological data. Specifically, we study which differences in data features (such as frequency, amplitude or signal-to-noise ratio) are more salient to the models and therefore more likely to drive the state decomposition. Overall, we aim at providing guidance for an appropriate use of this type of analysis on one or two-channel neural electrophysiological data, and an informed interpretation of its results given the characteristics of the data and the purpose of the analysis.

Figure 1: Analysis workflow

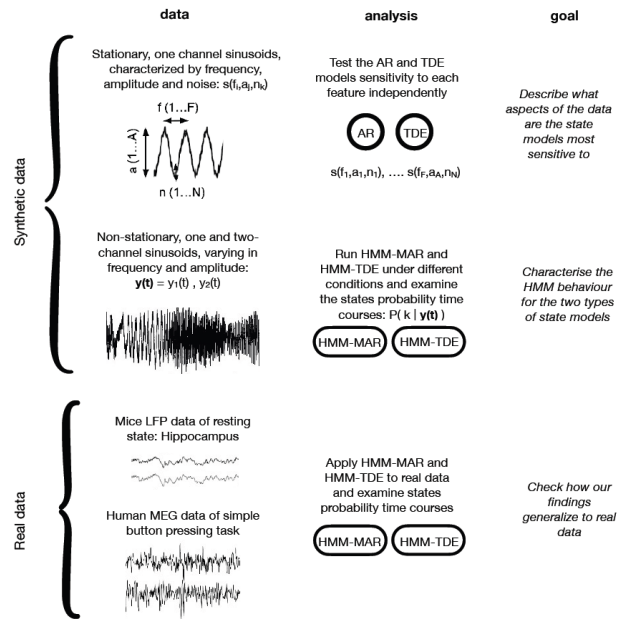
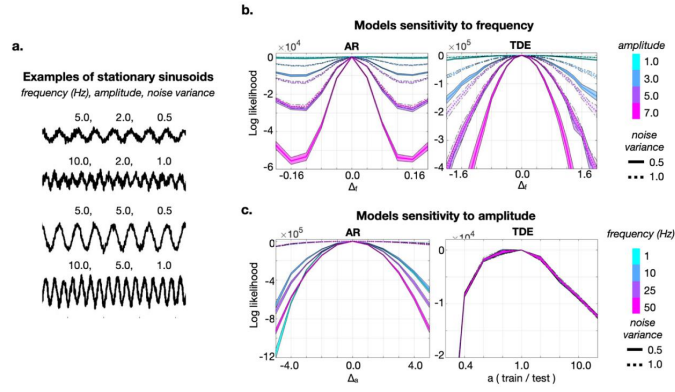


Figure 1: Scheme of the workflow, including data, analysis type and goals of each block.

**Figure 2:** Sensitivity analysis on the observation models



**Figure 2:** a. Example of signals used (stationary sinusoids), each defined by frequency, amplitude and noise variance. b. The plots show how the AR (left) and the TDE (right) models can tell apart two signals that differ only in frequency by an amount of  $\Delta f$  Hz (test frequency minus training frequency), for different values of their amplitude and of their noise content. The measure used is the logarithm of the likelihood ratio between train and test signal (given a fixed test signal and models trained on many training signals). Each solid line of the plot represents analyses for noise variance equal to 0.5, and each dotted line corresponds to noise variance equal to 1.0. By manipulating amplitude and noise variance, the plots show how the models perform for different signal to noise ratio (SNR) values. Here, AR order  $P=3$ , and TDE lags  $L=21$ , in steps of  $S=1$ ; signal length  $T=10$  seconds (25000 data points) c. AR and TDE sensitivity to amplitude, expressed as  $\Delta a$  for the AR model (training amplitude minus test amplitude) and as training amplitude in proportion to the target test amplitude (denoted as *train/test*) for the TDE model, for different values of frequency and of noise variance. Order, lags and signal length set as in b.

**Figure 3:** HMM experiments on one-channel non-stationary data

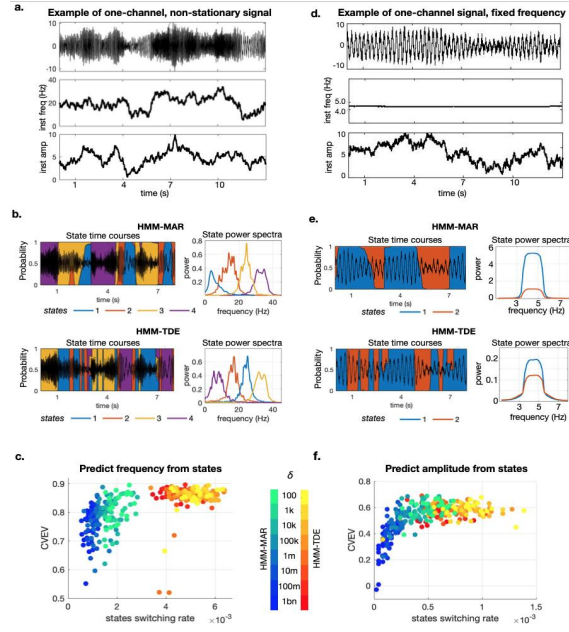


**Figure 3:** **a.** Example of signal varying in frequency (instantaneous frequency shown in the middle panel) and amplitude (instantaneous amplitude in the bottom panel). **b.** Example of the probabilistic state time courses and state power spectra of HMM-MAR and HMM-TDE applied to the signal in **a**. Here, transition probability matrix prior  $\delta = 10k$ , HMM-MAR order  $P=3$ , HMM-TDE lags  $L=15$  (in steps of  $S=3$ ). **c.** Cross validated explained variance of the HMM states predicting the ground truth frequency of non-stationary signals (like in **a**), for 20 repetitions of the experiment, for different values of the average state switching rate, manipulated via  $\delta$  (order and lags set as in **b**). **d.** Similarly to **a**: example of a synthetic signal varying mostly in amplitude. **e.** Example of probabilistic state time courses and state power spectra of HMM-MAR and HMM-TDE applied to the signal in **d**. Here,  $\delta = 10k$ ,  $P=3$ ,  $L = 15$ ,  $S=3$ . **f.** Cross validated explained variance of the HMM states predicting the ground truth amplitude of the signals as a function of the average state switching rate (varying  $\delta$ , order and lags set as in **e**), for 20 repetitions of the experiment.

**Figure 4:** HMM experiments on two-channel data with periodic coherence

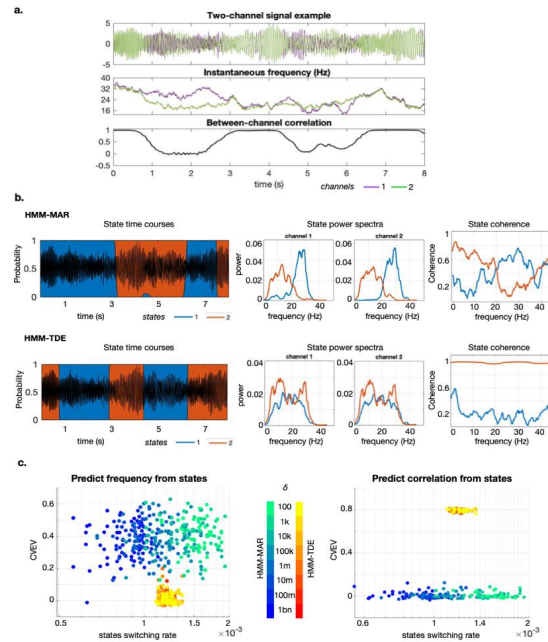


**Figure 4:** a. Example of the synthetic signals; instantaneous frequency is shown in the middle panel, and instantaneous correlation in the bottom panel. b. On the left, examples of the state time courses of HMM-MAR (top panel) and HMM-TDE (bottom panel) applied to the signal in a; shown also the corresponding state power spectra (middle) and coherence (right). Here,  $\delta = 10k$ , HMM-MAR order  $P=3$ , and the HMM-TDE lags  $L=15$ , with  $S=3$ . c. Cross validated explained variance (CVEV) of the HMM states predicting the ground truth instantaneous frequency of the channels (average explained variance across channels, left) and channel correlation (right) for 10 repetitions of the experiment and for different values of the state switching rate, manipulated through  $\delta$ . Order and lags set as in b.

**Figure 5: Analysis on LFP data**

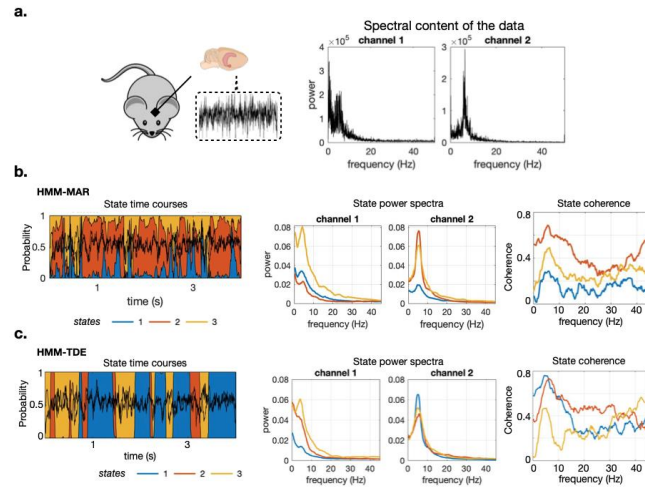


**Figure 5. a.** LFP data, with two LFP channels (chosen such that their activity was not very correlated) from the hippocampus of a mouse during resting state, downsampled to 250 Hz and the spectral content of the two channels. **b.** Example of HMM-MAR state time courses, as well as the state power spectra and the state coherence. **c.** Similar to **b.**, for HMM-TDE. The models are trained on 30 mins of data with three states (here, HMM-MAR order  $P=5$ , HMM-TDE, lags  $L=15$ ,  $S=3$ ,  $\delta=100k$ ).

**Figure 6:** Analysis on MEG data

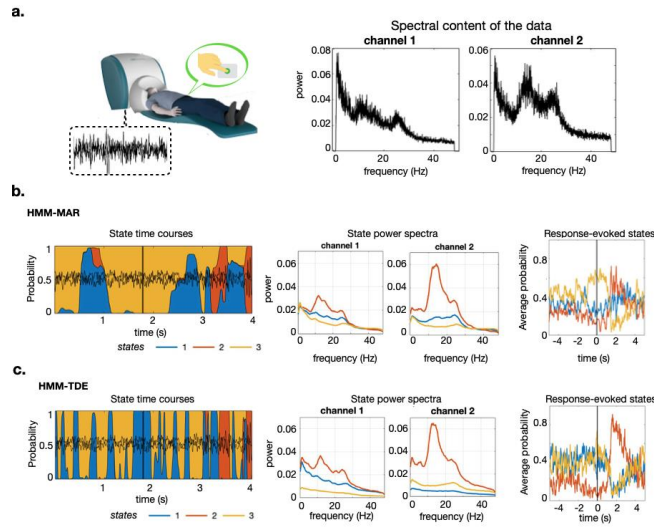


**Figure 6. a.** The data for this analysis are 2 MEG channels from the motor cortex of 8 (human) subjects who performed a simple finger tapping task. Data were downsampled to 200 Hz and band-filtered between 1 and 48 Hz. The spectral content of the two channels is also shown. **b.** Example of HMM-MAR state time courses, around a button press, marked by a black vertical line (left); the corresponding state power spectra (middle); and the probability of states around the button press (response-evoked state probability, rightmost panel). **c.** Same as in **b.**, for the HMM-TDE model. The models are trained on 20 mins of recordings with three states. For the HMM-MAR we used order  $P=3$ , and for the HMM-TDE we used  $L=1$ , with  $S=1$ ;  $\delta=100000$  in both cases.

## **TITLE PAGE**

5 **Title:** *Dissecting unsupervised learning through hidden Markov modelling in electrophysiological data*

**Running title:** *Analysis of HMM behaviour on brain data*

10 **Authors:** Laura Masaracchia<sup>a</sup>, Felipe Fedes<sup>b</sup>, Mark W. Woolrich<sup>c</sup> and Diego Vidaurre<sup>a, c</sup>

a - Center of Functionally Integrative Neuroscience, Department of Clinical Medicine, Aarhus University, Aarhus 8000, Denmark

15 b - Center for Proteins in Memory, Department of Biomedicine, Aarhus University, Aarhus 8000, Denmark

c - Oxford Centre for Human Brain Activity, Psychiatry Department, Oxford University, Oxford OX3 7JX, UK

20 **Corresponding Author:** Laura Masaracchia, [laurama@cfin.au.dk](mailto:laurama@cfin.au.dk)

**Acknowledgments:** DV is supported by a Novo Nordisk Foundation Emerging Investigator Fellowship (NNF19OC-0054895) and an ERC Starting Grant (ERC-StG-2019-850404). MWW's research is supported by the [NIHR](#) Oxford Health Biomedical Research center, the Wellcome Trust (106183/Z/14/Z, 215573/Z/19/Z), the New Therapeutics in Alzheimer's Diseases (NTAD) study supported by UK MRC, the Dementia Platform UK (RG94383/RG89702) and the EU-project euSNN (MSCA-ITN H2020-860563).

30 **Conflict of interest statement:** All authors declare that they have no conflicts of interest.

35

40

45

# Dissecting unsupervised learning through hidden Markov modelling in electrophysiological data

50 Laura Masaracchia<sup>\*a</sup>, Felipe Fredes<sup>b</sup>, Mark W. Woolrich<sup>c</sup> and Diego Vidaurre<sup>a, c</sup>

a - Center of Functionally Integrative Neuroscience, Department of Clinical Medicine, Aarhus University, Aarhus, Denmark

b - Center for Proteins in Memory, Department of Biomedicine, Aarhus University, Aarhus, Denmark

55 c - Oxford Centre for Human Brain Activity, Psychiatry Department, Oxford University, Oxford, UK

\*Corresponding author: [laurama@cfin.au.dk](mailto:laurama@cfin.au.dk)

60 **Acknowledgments:** DV is supported by a Novo Nordisk Foundation Emerging Investigator Fellowship (NNF19OC-0054895) and an ERC Starting Grant (ERC-StG-2019-850404). MWW's research is supported by the NIHR Oxford Health Biomedical Research center, the Wellcome Trust (106183/Z/14/Z, 215573/Z/19/Z), the New Therapeutics in Alzheimer's Diseases (NTAD) study supported by UK MRC, the Dementia Platform UK (RG94383/RG89702) and the EU-project euSNN (MSCA-ITN H2020-860563).

## ABSTRACT

70 Unsupervised, data-driven methods are commonly used in neuroscience to automatically decompose data into interpretable patterns. These patterns differ from one another depending on the assumptions of the models. How these assumptions affect specific data decompositions in practice, however, is often unclear, which hinders model applicability and interpretability. For instance, the hidden Markov model (HMM) automatically detects characteristic, recurring activity patterns (so-called *states*) from time series data. States are defined by a certain probability distribution, whose state-specific parameters are estimated from the data. But what specific features, from all of those that the data contain, do the states capture? That depends on the choice of probability distribution and on other model hyperparameters. Using both synthetic and real data, we aim at better characterising the behaviour of two HMM types that can be applied to electrophysiological data. Specifically, we study which differences in data features (such as frequency, amplitude or signal-to-noise ratio) are more salient to the models and therefore more likely to drive the state decomposition. Overall, we aim at providing guidance for an appropriate use of this type of analysis on one or two-channel neural electrophysiological data, and an informed interpretation of its results given the characteristics of the data and the purpose of the analysis.

85 **Keywords:** Unsupervised learning, hidden Markov models, computational modelling, electrophysiological data, data analysis, neuroscience.

90

## 1. INTRODUCTION

In empirical neuroscience, we often use supervised methods of analysis to investigate the mechanistic underpinnings of cognitive processing. These are supervised in the sense that they assume a certain preconception of the patterns of interest, and search for their expressions in the data accordingly. Some examples are decoding analysis (King and Dehaene, 2014; Quiroga and Panzeri, 2009; Haynes and Rees, 2006), analyses of evoked response potentials (ERP; Picton *et*

100 *al.*, 2000; Herrmann and Knight, 2001; Kotchoubey, 2005) and methods to characterise oscillations (Buzsáki and Draguhn, 2004; Donoghue *et al.*, 2020; Donoghue *et al.*, 2022). Overall, supervised approaches rely on prior knowledge and definitions of the features of interest, which could potentially be incomplete or imprecise.

105 An alternative approach is the use of data-driven, unsupervised models to automatically extract patterns from brain data without a prior definition of such patterns. For example, a clustering algorithm run on the time series data would automatically find a collection of patterns that was not defined beforehand, and it is then the researcher's task to determine what these patterns might mean neurobiologically. While unsupervised methods are potentially less biased and therefore can have a better chance of finding new information, they may also be more difficult to interpret. For this reason, it is important to, at least, have a clear understanding of what elements in the data are more salient for the chosen unsupervised algorithm, in order to elucidate what a given decomposition is really capturing.

110 We focus on the Hidden Markov Model (HMM; Rabiner, 1989), that have been used to investigate various domains, such as resting state dynamics in wakefulness (Vidaurre *et al.*, 2017; Vidaurre *et al.*, 2018; Karapanagiotidis *et al.*, 2020; Baker *et al.*, 2014; Shappel *et al.*, 2019) and sleep (Stevner *et al.*, 2019), perceptual processing (Vidaurre *et al.*, 2019), memory replay (Higgins *et al.*, 2021) and higher-order cognition (Baldassano *et al.*, 2018). These studies are examples of how the HMM can automatically identify patterns of activity (so-called *states*) without the need of providing beforehand a stringent, explicit definition of what would constitute a meaningful pattern. But what aspects of the data are more salient to the model, i.e., what is really driving the state inference? That depends on the choice of the observation model, which is the probability distribution used to represent the states. Two different observation models might have different views of saliency (meaning that different modulations in the data are considered more important for different models), and therefore behave differently. Often, the choice of one model over another is left to trial and error. While empirical comparisons have been made in the past between different observation models for specific purposes (Quinn *et al.*, 2019), no study has rigorously investigated what specific features within the data are the different state definitions most sensitive to. We reason that a better understanding of the various alternatives is important to fully leverage the benefits of this type of unsupervised analysis and interpret their outputs.

130 Specifically, focusing on raw, low-dimensional (one or two channels) electrophysiological data, we explore two types of HMM: the HMM-MAR, where the states are multivariate autoregressive models (Vidaurre *et al.*, 2016); and the HMM-TDE (time-delay embedded), where the states correspond to autocovariance patterns in the signal (Vidaurre *et al.*, 2018). High-dimensional data, where the focus is on finding complex network-level modulations (and where the HMM-TDE is preferred due to the difficulties of the HMM-MAR to scale up —see Vidaurre *et al.*, 2018) are not considered here.

140 We first use synthetic data to investigate how sensitive the two observation models are to variations in frequency, amplitude, signal-to-noise ratio, and amount of data. Then, we analyse how these characteristics affect the estimation of the states in the HMMs. Finally, we examine the behaviour of the models on two different real data modalities, LFP from mice in resting state and MEG from humans performing a simple motor task. In summary, our results show what to expect from the HMM states according to data conditions and analysis settings. On these grounds, we provide some recommendations on which model to use depending on the data and the purpose of the analysis.

## 2. MATERIALS & METHODS

150 Using both real and simulated electrophysiological data, this study investigated the behaviour of  
two varieties of the HMM: the HMM-MAR (Vidaurre *et al.*, 2016) and the HMM-TDE (Vidaurre *et*  
*al.*, 2018). First, a sensitivity analysis on the observation models (MAR and TDE) was conducted,  
with respect to different data features and model hyperparameters. Secondly, the full HMMs'  
155 behaviour was assessed, using both synthetic and real electrophysiological data: LFP data from  
a mouse hippocampus (during wakeful resting) and MEG data of human subjects performing a  
simple button press task. A schematic of the study is shown in **Figure 1**.

### 2.1 Data

#### 160 2.1.1 Synthetic data

##### Synthetic, stationary, one-channel signals

We tested the stand-alone observation model sensitivity to different data features using single-  
165 sinusoidal (stationary) signals, defined by frequency  $f$ , sampling frequency  $F$ , signal length  $T$ ,  
amplitude  $a$ , plus some random Gaussian noise, parametrised by its variance  $v$ . While  $F$  was kept  
constant, a range of values was established for the other features, and stationary sinusoids  
were sampled with all the combinations of the different features' values. Specifically,  $f$  ranged  
170 from 0.5 to 45 Hz in steps of 0.02 Hz,  $a$  ranged between 0.5 and 10.5 (arbitrary units) in steps of  
0.5 for the MAR model, and between 0.5 and 25 in multiplicative steps (proportions of 5.0) for the  
TDE model,  $v$  was either 0.5 or 1.0, and  $T$  was 2, 5, 10 or 15 seconds.  $F$  was 250 Hz in all cases  
(see **Figure 2a** for some examples).

##### Synthetic, non-stationary, one-channel signals

175 We used synthetic, non-stationary, one-channel signals to explore how the HMM-MAR and HMM-  
TDE segmented the time series into states visits (i.e., how they defined states and assigned a  
state probability per data point). The non-stationary oscillatory signals were created in such a way  
that signals had time varying frequency (ranging between 0.1 and 45.0 Hz) and amplitude  
180 (ranging between 0.1 and 10.0). Note that this generative model is more general (i.e., with more  
degrees of freedom) than the HMM, which assumes signals with quasi-stationary periods of  
sustained oscillations. Specifically, the instantaneous frequency  $f(t)$  and instantaneous  
amplitude  $a(t)$  were generated as two independent random walks, bounded within the chosen  
frequency and amplitude ranges, and where the step size at each time point was drawn from a  
185 normal distribution. The non-stationary, oscillatory signals were synthesized as a unique session  
of  $T=50000$  data points, with sampling frequency  $F=250$  Hz, and noise variance  $v=1.0$   
(see **Figure 3a** for an example), and then fed to the HMMs. The simulated session was  
then divided into  $N=100$  trials of  $t_N=500$  timepoints each, to ease a cross-validation scheme for  
our prediction analysis (see **Section 2.3.2** for details).

190

##### Synthetic, non-stationary, two-channel signals

The HMMs were then tested on two-channel data showing time-varying between-channel  
195 coherence (to simulate simplified functional connectivity in the data). In particular, the two  
periodically coherent channels,  $x_1$  and  $x_2$ , were generated combining three independent, non-  
stationary, one-channel signals (sampled as detailed above)  $a$ ,  $b$  and  $c$ , as follows:

$$x_1(t) = [1 - \rho(t)]a(t) + \rho(t)c(t) , \quad x_2(t) = [1 - \rho(t)]b(t) + \rho(t)c(t) ,$$

200 where  $\rho(t)$  modulates the channels similarity at each time point, and was generated as a smooth square wave (between 0 and 1) with a 4 seconds (1000 points) period. This way, when  $\rho(t) = 1$  the two channels were equal to  $c(t)$  and therefore maximally coherent; however, when  $\rho(t) = 0$ , the two channels corresponded, respectively, to  $a(t)$  and  $b(t)$ , which were independently generated—but, crucially, not forced to be strictly uncorrelated, and hence they could still exhibit  
205 some residual correlation due to sampling variability. In this sense,  $\rho(t)$  was not a real measure for coherence, and we adopted instead the two channels' instantaneous empirical correlation  $r(t)$ , computed within a sliding window, as a surrogate measure of the ground-truth channels' coherence. The sliding window's size was chosen such that  $r(t)$  matched best  $\rho(t) = 1$ , i.e., when the two channels were actually the same signal, and their ground-truth coherence was known.  
210 Again, the data were generated as a continuous session of  $T=50000$  points (see example in **Figure 4a**), fed to the HMMs and then reshaped into  $N=100$  trials of  $t_N = 500$  points for the prediction analysis (see below).

### 215 **2.1.2 Real data**

#### **LFP data**

Wakeful resting state data were collected for 30 mins from a mouse's hippocampus, using intracranial (Neuropixel) recordings. We used two channels from the array of 385 neuropixel  
220 electrodes for our tests. These data are part of a yet unpublished dataset, but are available upon request.

In detail, C57BL6/J male mice were first anesthetized with isofluorane (1% in oxygen) and placed in a stereotaxic apparatus (Kopf, California). A craniotomy was performed, centered in AP: -3.2, ML: 3 coordinates from bregma. Then, a head fixation crown (Neurotar, Helsinki) was implanted and secured with UV curating cement. Finally, a ground wire was implanted in the superficial layers of the cerebellum. The exposed craniotomy was covered with silicone (Kwik-cast, WPI) for protection. Meloxicam (5 mg/kg) were injected subcutaneously for three days after the surgery for pain and inflammation relief. The animals were allowed to recover for five days with food and  
230 water *ad libitum*. Then they were handled twice a day and placed in the head fixing apparatus for increasing times (10 mins to 40 mins), for 6 days to reduce stress. In the 7<sup>th</sup> day, the animal was head-fixed, and the silicone removed from the craniotomy. Then, a Neuropixel 2b probe was inserted at 1 $\mu$ m/second. The probe was inserted a total of 4 mm corresponding to the first 385 recording sites of the probe. These spanned secondary visual cortex and ventral dentate gyrus.  
235 After 15 mins, LFP data was filtered (0.5-1000 Hz), amplified and digitized (2.5 kHz). Data was acquired for 30 mins, while the animal was in resting state, in darkness. For our analyses, we used 2 channels, chosen such that their activity was not very correlated, from the hippocampus of one mouse and downsampled the data to 250 Hz.

#### 240 **MEG data**

The MEG data used in this study were collected by O'Neill *et al.* (2015), where eight subjects were instructed to perform a button press with the index finger of their left hand using a keypad, roughly every 30 seconds and without counting the time in between button presses. Total  
245 scanning time was 1200 seconds per subject. The data were acquired using a 275 channel CTF whole-head system (MISL, Conquitlam, Canada) at a sampling rate of 600 Hz with a 150 Hz low pass anti-aliasing filter. Synthetic third order gradiometer correction was applied to reduce external interference. The data were converted to SPM8 and downsampled to 200 Hz. We used

250 the same preprocessing pipeline as in Vidaurre *et al.*, (2016). After the removal of artifacts related  
to eye-blink and heartbeat with Independent Component Analysis (ICA; Hyvärinen and Oja,  
2000), the data were band-pass filtered between 1 and 48 Hz, and source-reconstructed to the  
two primary motor cortices (M1).

## 255 **2.2 Models**

### **2.2.1 The Hidden Markov Model (HMM)**

260 The Hidden Markov Model (HMM) is a family of probabilistic models describing time series data  
as a sequence of  $K$  states (Rabiner, 1989). Each state corresponds to a different probability  
distribution (also known as observation model), belonging to a pre-specified family of probability  
distributions (e.g., Gaussian). The HMM inference estimates, in a data-driven fashion, the state  
parameters, the probability of each state being active per time point (*state time course*), the  
265 transition probability matrix (i.e., the probability of changing from one state to another, and of  
remaining in the same state), and the initial state probabilities (i.e., the probability of each state  
at trial start).

Here two types of HMM were explored, the HMM-MAR (Vidaurre *et al.*, 2016) and the HMM-TDE  
(Vidaurre *et al.*, 2018), each with a different observation model (see below). Both are implemented  
270 in the HMM-MAR toolbox, publicly available on GitHub<sup>1</sup>. In our analyses, we manipulated:

- The respective model hyperparameters: the order  $P$  for the HMM-MAR and the lags  
structure for the HMM-TDE, defined by the width  $L$  and the inter lags steps  $S$  (see below for  
275 definitions).
- The prior probability of remaining in the same state as opposed to moving to another state,  
parametrised by the Dirichlet distribution concentration parameter<sup>2</sup>, denoted as  $\delta$ .
- The number of states  $K$ .

280 We used non-parametric estimations of the state spectra and coherence<sup>3</sup>.

### **2.2.2 Observation Models**

#### **Multivariate Autoregressive (MAR) observation model**

285 Given a multichannel time series  $\mathbf{y}$ , the MAR model model the signal at each data point  $\mathbf{y}_t$  as a  
linear combination of previous time points ( $\mathbf{y}_{t-1}, \dots, \mathbf{y}_{t-p}$ ), given the generative model

$$P(\mathbf{y}_t) \sim N\left(\sum_{j=1}^P \mathbf{y}_{t-j} \mathbf{W}_j, \sigma^2\right), \forall t$$

290 where  $\mathbf{W}$  are the autoregressive coefficients,  $\sigma^2$  is the noise variance, and  $P$  is the autoregressive  
order, which determines the spectral resolution of the model. For a given choice of  $P$ , Bayesian  
inference is used here to estimate  $\mathbf{W}$  and  $\sigma^2$ , given the data.

295 In the HMM-MAR, each state's probability distribution is represented by a set of coefficients  $\mathbf{W}^{(k)}$   
per state  $k$ , as per:

---

<sup>1</sup> <https://github.com/OHBA-analysis/HMM-MAR>

<sup>2</sup> In the HMM-MAR toolbox, this is specified with the *DirichletDiag* option.

<sup>3</sup> Function *hmmspectramt()* in the toolbox.

$$P(\mathbf{y}_t | x_t = k) \sim N\left(\sum_{j=1}^P y_{t-j} W_j^{(k)}, \sigma^2\right), \forall t,$$

300 where  $x_t$  is a hidden variable indicating the state active at time point  $t$ ,  $x_t$  is also estimated from the data.

When dealing with one-channel signals, we will just refer to the MAR model as autoregressive model or AR (and, correspondingly, HMM-AR).

### 305 **Time-Delay Embedded (TDE) observation model**

310 Instead of modelling the probability of observing every time point of the data, the TDE models the autocovariance of the signal around time point  $t$ . The relevant hyperparameter here is the lag structure, defined by  $L$  (the width of the signal's window to consider at each time point) and  $S$  (how many steps separate each lag), as per  $[-L, -L+S, \dots, 0, \dots, L-S, L]$ . Mathematically, given the expansion  $\mathbf{Y}_t = (\mathbf{y}_{t-L}, \dots, \mathbf{y}_t, \dots, \mathbf{y}_{t+L})$ , the model is defined as Gaussian:

$$P(\mathbf{Y}_t) \sim N(0, \Sigma), \forall t,$$

315 where  $\Sigma$  is the autocovariance of the signal encoding linear relations across regions and time points within the window around  $t$ . The HMM-TDE is then defined as

$$P(\mathbf{Y}_t | x_t = k) \sim N(0, \Sigma^{(k)}).$$

## 320 **2.3 Analyses**

325 Two types of analysis were performed: first, a sensitivity analysis on the observation models with respect to data features, as well as amount of training data and model hyperparameters; and second, a prediction analysis on the full HMM distributions assessing the generality of the estimation of the content of the states, as well as a permutation testing analysis to confirm the results.

### **2.3.1 Sensitivity analysis on the observation models**

330 The sensitivity of the two observation models, MAR and TDE, to different data features was tested: specifically, we assessed how the manipulation of frequency, amplitude and noise variance, as well as amount of data and model hyperparameters (the order for the MAR  $P$  and the TDE lags manipulated by  $L$ , while  $S$  was kept to 1) affected the estimations of  $\mathbf{W}$  and  $\Sigma$  respectively. Two independent sets of synthetic stationary data (as described in **Section**

335 **2.1.1**) were generated, both containing signals with all the above-mentioned feature combinations. One set was used for training the models and one for testing them. Since this analysis involved one-channel stationary signals, we will refer to the MAR model as AR. For every signal  $\mathbf{y}$  from the training set, the model coefficients  $\mathbf{W}$  (for the AR) and  $\Sigma$  (for the TDE) were estimated. We will refer to these as  $\mathbf{W}(\mathbf{y})$ , and  $\Sigma(\mathbf{y})$ . The trained models were then tested on one

340 target signal  $\mathbf{z}$  from the test set. The capacity of the models to describe this test signal was measured by means of the log-likelihood ratio (of trained vs tested signal): this gave an indication of how similar training and test signals were, according to the trained models. Being model-dependent, the log-likelihood ratio expresses the sensitivity of each model with respect to each feature.

345

For the AR model, the likelihood of the target test signal  $\mathbf{z}$  to be distributed as a training signal  $\mathbf{y}$  is:

$$L(\mathbf{z}|\mathbf{W}(\mathbf{y})) = \prod_t L(z_t | \mathbf{W}(\mathbf{y})) = \prod_t \frac{1}{\sqrt{2\pi\sigma^2}} \exp\left[-\frac{(z_t - \mu_t)^2}{2\sigma^2}\right],$$

350 where  $\mu_t = \sum_{j=1}^P z_{t-j} W(y)_j$  is the prediction from the autoregressive model, and  $\sigma$  is the noise standard deviation, also estimated from the data.

For the TDE model, given  $\mathbf{Z}_t = (z_{t-L}, \dots, z_t, \dots, z_{t+L})$ , the likelihood of  $\mathbf{Z}_t$  to be distributed according to  $N(0, \Sigma(\mathbf{y}))$ , for a training signal  $\mathbf{y}$ , is:

355

$$L(\mathbf{Z}_t | \Sigma(\mathbf{y})) = \frac{1}{\sqrt{2\pi|\Sigma(\mathbf{y})|}} \exp\left[-\frac{1}{2} \mathbf{Z}_t^T \Sigma(\mathbf{y})^{-1} \mathbf{Z}_t\right],$$

where  $|\Sigma(\mathbf{y})|$  indicates the determinant of  $\Sigma(\mathbf{y})$ . Then, the likelihood across time points becomes:

360

$$L(\mathbf{z}|\Sigma(\mathbf{y})) = \prod_t L(\mathbf{Z}_t | \Sigma(\mathbf{y})).$$

Finally, considering the likelihood of target signal  $\mathbf{z}$  to be parametrised by a model trained on  $\mathbf{z}$  (i.e., a training signal with the same features),  $L(\mathbf{z}|\mathbf{W}(\mathbf{z}))$  and  $L(\mathbf{z}|\Sigma(\mathbf{z}))$ , the log-likelihood ratios are defined as:

365

$$\log \left[ \frac{L(\mathbf{z} | \mathbf{W}(\mathbf{y}))}{L(\mathbf{z} | \mathbf{W}(\mathbf{z}))} \right] \text{ and } \log \left[ \frac{L(\mathbf{z} | \Sigma(\mathbf{y}))}{L(\mathbf{z} | \Sigma(\mathbf{z}))} \right].$$

The log likelihood ratio is therefore a measure of the precision of the model in describing the test signal, given the training signal. If the log likelihood ratio of the model trained on  $\mathbf{y}$  vs  $\mathbf{z}$  is low (i.e. a large negative number), then the parameters of the model fitted to  $\mathbf{y}$  do not describe well the test data  $\mathbf{z}$ , and, consequently, the two signals are regarded as different according to the assumptions of the model; on the other hand, if the log likelihood ratio is close to zero, both the models trained on  $\mathbf{y}$  and  $\mathbf{z}$  describe well the test data and, therefore, that the two signals cannot be distinguished given the model definition and assumptions.

375

### 2.3.2 HMM analyses on synthetic data

The previous analyses were designed to compare the observation models as stand-alone distributions. Next, these were assessed within the HMM framework. Specifically, the HMM states were assessed by regressing the state time courses on the ground-truth data features — instantaneous frequency  $f(t)$ , amplitude  $a(t)$  and between-channel correlation  $r(t)$ . In order to use a cross validation scheme, the data, simulated as a unique session of  $T=50000$  points, were partitioned into trials of equal length. The cross validation was hence performed at the trial level, grouping the trials into 10 folds (using 9 for training and the remaining 1 for testing, in turns).

380

385 This yielded a measure of accuracy —cross-validated explained variance (CVEV)— per feature, describing how well the HMM states captured that feature. The accuracy of the models in capturing each feature was tested as a function of the observation model hyperparameters and of the prior probability of remaining in the same state, hyperparametrised by  $\delta$  (see above). To confirm the reproducibility of the results, each analysis was repeated 20 times.

390

A permutation testing analysis was conducted (10000 permutations) to further validate the effects of the prediction analyses, where the null hypotheses are of the sort of “the HMM states do not capture amplitude”. The permutations were also performed across trials.

### 395 **2.3.3 HMM analyses on real data**

The two HMMs were also tested on LFP and MEG real data, comparing the frequency properties of the states. For the MEG data, the state temporal information was also contrasted to the available task data.

400

## **2.4 Code accessibility**

All the code used for the generation of synthetic data and for the analysis of both synthetic and real data will be available upon publication on Github<sup>4</sup>.

405

## **3. RESULTS**

### 410 **3.1 Observation models sensitivity**

In the first part of this study, a sensitivity analysis was conducted on the two HMM observation models (autoregressive and TDE), with respect to data characteristics and model hyperparameters. The models were trained and tested on synthetic, stationary sinusoids (described in **Section 2.1.1**, see examples in **Figure 2a**), and their sensitivity measured by the log likelihood ratio of train vs. test signal, which we can interpret as a measure of how well the models could identify signal differences (see **Section 2.3.1**).

415

To test the model sensitivity to frequency, the models were trained on signals that only differed in frequency (i.e., with a fixed amplitude and noise variance). We then selected a given target test frequency and tested the models (trained for multiple frequencies) on the test signal, which had the same amplitude and noise variance as the training signals. The procedure was repeated to test different amplitude and noise values (**Figure 2b**). The TDE model showed lower frequency resolution than the AR model (note the different x-axes scales in the plots). Generally, decreasing amplitude and increasing noise had a similar effect on the sensitivity of the models to frequency. For the AR model, signal-to-noise ratio (SNR), rather than amplitude or noise variance as separate factors, affected its frequency resolution: that is, the smallest detectable frequency difference depended on the signals' SNR. This intuition can be verified analytically by proving that the coefficients of two models trained on signals with different amplitude and noise variance, but same SNR value, are the same (see **Appendix**).

420

425

430

To test the model sensitivity to amplitude, the same procedure detailed above was adopted: the models were trained and tested on signals that only differed in amplitude, for some fixed values of frequency and noise variance (**Figure 2c**). While the AR model clearly distinguished the full range of amplitudes tested, it was more difficult for the TDE to distinguish training and test signal, especially when the training amplitude was higher than the test one. Because of this, we tested a wider range of amplitude differences for the TDE model, where we used multipliers of the target test amplitude as training amplitudes (for the AR model, the different training amplitudes were

435

---

<sup>4</sup> [https://github.com/LauraMasaracchia/HMM\\_explore](https://github.com/LauraMasaracchia/HMM_explore)

linearly spaced). Overall, amplitude resolution was not affected by frequency, as the model relative performance was similar for all tested frequencies.

440 Frequency and amplitude resolution of the models were further investigated by varying the amount of training data (manipulating signal length) and the model hyperparameters —see **Supplementary Figure 1**. Briefly, more training data induced a higher resolution on frequency in both models, and a higher sensitivity to amplitude in the AR model. Also, a larger lag window in the TDE model increased frequency resolution. Neither a higher amount of data, nor a bigger lag window significantly changed the TDE sensitivity to amplitude. As for the AR model, since an autoregressive order of 3 can already capture one fundamental frequency, and because in this particular case the data only had one frequency, an increase in the autoregressive order did not change the model performance. That is, while a higher autoregressive order could explain more complex, multi-frequency spectral patterns, it does not improve the resolution of a single frequency.

In summary, the AR model accurately described stationary sinusoids with sufficiently high SNR and showed high frequency resolution, which was also influenced by the amount of training data. The AR model was comparably less sensitive to amplitude than to frequency, and also amplitude resolution was influenced by the amount of training data. On the other hand, the TDE model showed a lower frequency resolution than the AR. This resolution was modulated by the lag hyperparameter and by the amount of training data. Finally, the TDE model was less sensitive to differences in amplitude, and, unlike the AR, its sensitivity was not symmetric (see **Figure 2c**); this is because, for the TDE (i.e., for the Gaussian distribution), the log-likelihood function (unlike the probability density function) is not symmetric with respect to the scale. Manipulations in lags or amount of training data did not significantly change this behaviour.

## 465 **3.2 HMM inference**

Next, the HMM-MAR and HMM-TDE capacity to represent dynamic changes in the signal was investigated, using synthetic, non-stationary signals with time-varying frequency, amplitude and functional connectivity (as described in **Section 2.1.1**).

### 470 **3.2.1 Detection of changes in frequency and amplitude**

The HMM-MAR and the HMM-TDE were first tested on single-channel signals with time-varying frequency and amplitude. As mentioned in **Section 2.1.1**, the generative model of the signals, unlike the HMM's, does not assume quasi-stationary periods of sustained oscillations, and is, therefore, more general. While we could have generated data that followed the assumptions of the HMM, real electrophysiological data is likely to not follow these assumptions, so we opted for a more assumption-free generative model. In detail, one-channel, non-stationary signals were fed to the HMMs and the resulting state time courses (i.e., the probability of each state being active at each time point) were subsequently analysed. In particular, standard regression was used to predict the frequency and amplitude time courses from the state time courses, in a cross validated fashion. The prediction analysis was performed varying the hyperparameter  $\delta$  (related to the prior probability of remaining in the same state, which influences the state switching rate; see above), as well as the order for the HMM-MAR and the lags for the HMM-TDE. The procedure was performed 20 times per configuration (see **Section 2.3.2**).

485 When the signals varied in frequency and amplitude (example signal in **Figure 3a**), both HMM-MAR and HMM-TDE clearly captured frequency changes, with each of their states representing

a different frequency band (**Figure 3b**). Our prediction analysis showed that, for fixed order and lags, the state switching rate affects model performance in capturing frequency (see **Figure 3c**, where order  $P=3$ , lags structure set to  $L=15$ , spaced in steps of  $S=3$ ): clearly, the models with faster switching rates (here, the HMM-TDE runs) could explain frequency variance better (up to 90%), meaning that they better matched the dynamics of the data. For comparison, a separate permutation analysis showed that randomly assigned states could explain only  $0.0132, \pm 0.0130$  of frequency variance (CI = 0.95,  $p < 0.0001$  for all models). The prediction analysis further showed that varying the model hyperparameters also had an influence on the performance of the models and on the state switching rate. More specifically, while  $\delta$  had a great influence on the HMM-MAR performance, widely modulating the state switching rate, the HMM-TDE performance and state switching rate were more affected by the lags manipulation than by  $\delta$  (see **Supplementary Figure 2a** for further details). None of the models could explain amplitude variance significantly better than randomly assigned states.

To further investigate the extent to which the HMM states could capture amplitude, the same analysis was performed on one-channel, non-stationary signals only varying in amplitude (a signal example is reported in **Figure 3d**). This time, coarse changes in amplitude could be captured using two states for each model (**Figure 3e**). The prediction analysis (now regressing the state time courses on the amplitude time course) for a fixed order and lag choices (as before,  $P=3$ ,  $L=15$ ,  $S=3$ ), showed that both models were able to detect amplitude changes in this scenario, but the extent to which they could do so depended on how well the state switching rate matched the ground-truth dynamics of the data (**Figure 3f**); for example, the extreme cases when the switching rate was close to zero (leftmost in the panel) corresponded to cases when one state dominated the entire decomposition, driving the CVEV to zero. This is in contrast with the previous analyses, where we examined the states as stand-alone distributions, and where the AR model was considerably better at capturing amplitude. The difference here is however at the level of the HMM inference, with certain HMM-MAR runs not being able to switch states at sufficient speed (or even collapsing to a single state) for some choices of  $\delta$ . For comparison, randomly assigned states explained  $0.0228 \pm 0.0227$  (CI = 0.95) of the signals' amplitude, yielding statistical significance for all decompositions that did not degenerate onto a single state. The complete analysis results can be found in **Supplementary Figure 2b**.

We also explored the HMM-MAR and HMM-TDE inference for a higher number of states, using signals that vary both in frequency and in amplitude (**Supplementary Figure 3**). When increasing the number of states, the HMM-MAR started capturing amplitude instead of only frequency (**Supplementary Figure 3c**). In contrast, endowing the HMM-TDE with more states resulted in a higher frequency band resolution, but no better sensitivity to amplitude (**Supplementary Figure 3f**).

In conclusion, both models were more sensitive to frequency than they are to amplitude, but they could also capture changes in amplitude when frequency was relatively constant and, in case of the HMM-MAR, when endowed with a higher number of states. How well the decomposition captured differences in amplitude and frequency depended on the temporal dynamics of the state time courses (i.e., the state switching rate) and how well they matched the underlying modulations in the data. As shown, the switching rate can be manipulated by modifying the observation model hyperparameters (e.g.  $L$  and  $P$ ) and the priors of the transition probability matrix ( $\delta$ ). In real scenarios, these hyperparameters could be tuned to access different temporal scales in the data.

As mentioned, these analyses may seem opposed to the previous section, where the MAR model showed to have a higher resolution in both frequency and amplitude. These findings can be reconciled by the fact that the MAR has a higher capacity to explain variance in the raw data, and

540 thus, when plugged into the HMM inference, might necessitate less state switching (specially,  
when overparametrised). That is, while a high-order single autoregressive model could potentially  
explain the data very well and therefore dominate the decomposition, the corresponding state  
time courses would not be effective to describe the time-varying facets of the data, which is what  
our CVEV metric precisely captures. While the same problem could occur for the HMM-TDE as  
545 well, it is less likely to happen because the number of effective parameters of the TDE (and  
therefore its sensitivity to the different features, as shown in the previous section) is lower.

### 3.2.2 Detection of changes in functional connectivity

550 Next, The HMM-MAR and the HMM-TDE were tested on synthetic two-channel, non-stationary  
signals with time-varying correlation across the entire frequency spectrum (see **Section 2.1.1**),  
which we will refer to as *broadband functional connectivity* (see **Figure 4a** for examples of signal  
and between-channel correlation). Again, a regression analysis was used to predict frequency  
and between-channel correlation from the state time courses, varying  $\delta$  and the observation model  
hyperparameters. The full experiment was repeated 10 times.

555 Here, the HMM-MAR primarily captured frequency information specific to the single channels,  
whereas the HMM-TDE was able to capture broadband functional connectivity, such that one  
state was assigned to the periods of highest correlation between the two channels and the other  
state to periods of lower correlation. This can be qualitatively observed in the state time courses  
560 (**Figure 4b**, leftmost panels) with respect to the channel correlations (**Figure 4a**, bottom panel),  
and in the estimation of the state power spectra (**Figure 4b**, middle panels) and  
the state coherence (**Figure 4b**, rightmost panels). The prediction analysis quantitatively  
corroborated this, showing that, for fixed order and lags (here,  $P=3$  and  $L=15$ , in steps of  $S=3$ ),  
565 varying  $\delta$  to manipulate the state switching rate did not change the HMM-TDE ability to capture  
broadband functional connectivity significantly (**Figure 4c**, right panel). This analysis also  
revealed that the HMM-MAR performance in predicting channel frequency was not very stable  
across runs (see how scattered the performance is along the y axis in **Figure 4c** left, regardless  
of the  $\delta$  parameter). For comparison, a permutation testing analysis resulted in randomly assigned  
570 states explaining  $0.0126 \pm 0.0125$  (CI=0.95) of the signal frequency variance, and  $0.0029 \pm$   
 $0.0027$  (CI = 0.95) of channel correlation variance; this means that the HMM-TDE did not perform  
significantly better than randomly assigned states in capturing frequency, and neither did the  
HMM-MAR in capturing broadband coherence.

575 We repeated the prediction analysis by varying the model hyperparameters (complete results in  
**Supplementary Figure 4**), showing again that the HMM-MAR performance and state dynamics  
were more affected by changes in  $\delta$  than HMM-TDE, which was most affected by the lag  
configuration.

580 But how can these results be reconciled with previous work where the HMM-TDE was  
successfully used to find states with distinct amounts of coherence in different frequency bands  
(for example, in Vidaurre *et al.*, 2018; Hirschmann *et al.*, 2020; Sharma *et al.*, 2021)? First, our  
analyses only used two states, inducing the models to focus on what was most salient to them.  
Note that while we could have used more states, the goal of this paper was precisely to  
585 characterise saliency. Since the HMM-TDE has less spectral detail than the HMM-MAR,  
broadband coherence resulted to be its most salient feature. Second, power and coherence are  
not independent. The HMM-MAR's states had different spectral signatures in coherence (**Figure**  
**4c**, right-bottom panel) also because they reflected their respective spectral signatures in power  
(**Figure 4c**, middle-bottom panel). We established before that the HMM-MAR has great sensitivity  
to frequency changes, which were present in this data (**Figure 4a**, middle panel) and hence

590 captured by the model. Altogether, our results do not imply that the HMM-TDE is unable to find spectral-specific changes in coherence, if they existed in the data, but that it would do so with less spectral detail than the HMM-MAR and it would instead prioritise broader frequency bands (or broadband coherence as in this example).

595 In summary, for bivariate signals exhibiting intermittent periods of high correlation, the first feature of focus for HMM-TDE was broadband connectivity, while the HMM-MAR was more sensitive to detailed frequency modulations and less to broadband connectivity.

### 600 3.2.3 Real data

We ran the two HMM were then on two real datasets: LFP data from mice in wakeful rest, and MEG data of humans performing a simple motor task (source-reconstructed onto two motor cortex parcels); see **Section 2.1.2** for details.

605 When applied to the LFP data, the state time courses of HMM-MAR and HMM-TDE were relatively well correlated, with an average correlation of 0.5, for the various tested configurations (number of states  $K=2,3,4$ , HMM-MAR order  $P=3,5,7,9$ ; HMM-TDE lags  $L=3,5,15,21$  in steps of 1,  $\delta = 1k, 10k, 100k, 1m, 10m$ ), indicating that the decompositions had overlapping properties; see **Figure 5a** for the spectral properties of the data. However, we found that the HMM-TDE inference exhibited much less uncertainty, namely that the HMM-TDE inference assigned very high probabilities to one state at each time point, while the HMM-MAR inference often had mixed probabilities; see state time courses and state properties of HMM-MAR and HMM-TDE in **Figure 5bc**. In particular, the HMM-TDE assigned probability of  $\sim 1.0$  to 90% of the time points on average, while for the HMM-MAR less than 20% of the points had a state with probability near to 1.0. This instability likely follows from the rich frequency content of high-quality LFP combined with the higher spectral sensitivity of the HMM-MAR.

620 When applied to MEG data (see **Figure 6a** for a spectral characterisation of the data), Vidaurre *et al.* (2016) previously showed that the HMM-MAR could capture task-related information without the model having prior knowledge of the task. Here, we ran the HMMs subject by subject and, similarly to Vidaurre *et al.* (2016), computed the response evoked state probability (i.e., the average probability of each state to be active within a window around the finger tapping event), alongside with the state power spectra. Since the channels were made orthogonal in order to correct for signal leakage (Brookes *et al.*, 2012) their coherence was greatly diminished (and not considered here). Like with the LFP data, the two HMM variants differed in the uncertainty of the state assignments, with the HMM-TDE assigning probabilities more sharply than the HMM-MAR (see **Figure 6b** and **c**, leftmost panels, for an example of the HMM-MAR and HMM-TDE state time courses). Still, both the HMM-MAR and HMM-TDE captured task information well; specifically, one state showed increasing probability of being active in the 2 seconds before the button press and has a drastic drop 1-2 seconds after, while another state had a specular behaviour, with very low probability of being active before the button press and a sharp increase 2-4 seconds after (see **Figure 6b** and **c**, rightmost panels, with the response-evoked state probabilities for HMM-MAR and HMM-TDE respectively). **Figure 6** shows the results for one exemplary subject; see **Supplementary Figure 5** for the other subjects.

635 In conclusion, here the state spectral properties were not as different between two models as in the synthetic simulations, but the HMM-TDE performed in a more stable way in the sense of having a higher certainty in the state time courses estimation.

640

## 4. DISCUSSION

In this study, focusing on electrophysiological data with one or two channels —both real and simulated, we explored in detail the behaviour of two types of HMMs: the HMM-MAR (Vidaurre *et al.*, 2016) and the HMM-TDE (Vidaurre *et al.*, 2018). We excluded other models that are instead run on amplitude time series derived from, for instance, a Fourier transform (Baker *et al.*, 2014). Using synthetic data, we first measured the sensitivity of the two observation models to different data features in a stand-alone manner. Then, we studied what dynamic aspects of the data drive the inference of the HMMs. Finally, we confronted the models with real MEG and LFP data.

650

Our sensitivity analysis of the standalone observation models showed that the MAR is more sensitive to frequency than it is to amplitude, and that it has a higher frequency resolution than the TDE observation model. We also found that it is harder for the TDE model to distinguish amplitude, and that its amplitude resolution is not symmetric (that is, the TDE is more sensitive to a testing amplitude that is higher than the training amplitude, and less sensitive to a testing amplitude that is lower than the training amplitude). The HMM analyses on single-channel signals with non-stationary properties showed that both the HMM-MAR and HMM-TDE preferentially capture changes in frequency when the signal is varying both in frequency and in amplitude. Except for degenerate solutions, the HMM-MAR could capture changes in amplitude when the signal did not vary much in frequency, or when the model was endowed with a high number of states. The HMM-TDE successfully captured amplitude reliably when the signal was only varying in amplitude, provided that the changes in amplitude were large enough. HMM-TDE showed generally more robust states dynamics than the HMM-MAR. Finally, we found that their performance depended on their hyperparameter configuration (on both the prior probability of remaining in the same state and on the model-specific hyperparameters). On two-channel synthetic data with transient periods of high functional connectivity (in the sense of between-channel correlation), we found that the HMM-MAR focuses first on representing frequency-specific changes at the expense of broadband functional connectivity (here, correlation), while the HMM-TDE clearly prefers focusing on broadband changes in functional connectivity above and beyond fine-grained fluctuations in the frequency content of the signals. Overall, we can conclude from these results that the HMM-MAR is the most appropriate model when the main goal of the analysis is detecting detailed changes in the frequency of the signal, or amplitude if the frequency is relatively stationary (for example as a result of filtering), while the HMM-TDE may be more appropriate in multi-channel data when the focus is on capturing spectrally-wide changes in functional connectivity, and, in general, when the MAR model is overparametrised and the inference collapses onto one single state.

675

While the balance in sensitivity to frequency and amplitude for the different models was unambiguously characterised in our single-channel experiments, it is important to note that our analyses are to some extent contingent to the generative model used to sample the data and its assumptions. In particular, our generative model (as described in **Section 2.1.1**) for pairs of channels did not explicitly model spectrally fine-grained changes in coherence, and instead manipulated spectrally broadband changes. Here, the HMM-TDE was clearly focusing mostly on changes in functional connectivity, but the HMM-MAR would have probably been more sensitive to connectivity if the ground-truth generative model were targeted at producing frequency-specific changes in coherence. While our generative model for sampling data is a reasonable approximation of actual empirical data in terms of their spectral properties, the sensitivity of the two models to connectivity will in the end be determined by how much explained variance in the

685

690 real data is attributable to changes in coherence vs. changes in power, and how this variance is spectrally distributed (i.e., coarse vs. fine-grained).

695 Having a greater sensitivity to the different features present in the data may however come at a price. Whereas the HMM-MAR is more sensitive to detailed spectral content than the HMM-TDE, this can also result in greater estimation volatility or observation model overfitting (where one state dominates most of the time series): for example, in the LFP experiment, the state time courses for the HMM-MAR often showed great uncertainty about which state is active at each time point, as opposed to the HMM-TDE, which was much more stable; also see **Figure 4c** (left panel), where the HMM-MAR's capacity to explain frequency showed large variability even when using similar hyperparameters. Volatility and variability can translate in lower reproducibility of the results, since small changes in the data are more likely to elicit larger changes in the resulting estimates. This has made the HMM-TDE the model of choice in several applications of the HMM in electrophysiological data (Khawaldeh *et al.*, 2022; Bai *et al.*, 2021; Higgins *et al.*, 2021; Sharma *et al.*, 2021). The cause of HMM-MAR greater instability is likely due to the nonlinearity of neural oscillatory signals, in the sense that the phase of the oscillations does not progress at linear steps, and, therefore, the shape of the wave is often irregular and asymmetric (that is, the instantaneous frequency of the signal varies irregularly from time point to time point; Huang *et al.*, 2009). Since both the TDE and the MAR models are linear, the only way to accurately model abrupt changes in instantaneous frequency is through the state time courses. For this reason, over-parametrised models with excessive sensitivity can be more volatile, and can even exhibit quick state switches within single oscillatory phase. Whereas these estimates are technically not incorrect, they lend to more complex interpretations.

## 715 **5. CONCLUSION**

715 Unsupervised methods of analysis provide a useful tool for discovery and are freer of researcher bias than other methods. But, at the same time, they can be a black box in the sense that we do not precisely know what aspects of the data they capture. Here we focused on an unsupervised method often applied to electrophysiological data, the hidden Markov model. Our aim is to characterise precisely what aspects in the data, such as frequency or amplitude modulations and functional connectivity, drive an HMM estimation. Using synthetic as well as real (LFP and MEG) data, we characterised the behaviour of two different types of HMM (the HMM-MAR and the HMM-TDE). In summary, we showed that both HMMs preferentially capture frequency modulations, but the HMM-MAR does it in more detail —this, in turn, results in more stable estimations for the HMM-TDE. For the same reason, the HMM-TDE is more effective in capturing functional connectivity modulations in relatively broad frequency bands. We note that the HMM is not a biophysical model, and different parametrisations or model choices offer just alternative perspectives of the data. On these grounds, none of these can be said to be biologically more or less valid than the others —only more or less practically useful given the characteristics of the data and the research goal.

735

740

## REFERENCES

- 745 Bai, Y., He, J., Xia, X., Wang, Y., Yang, Y., Di, H., Li, X., Ziemann, U. (2021). Spontaneous transient brain states in EEG source space in disorders of consciousness. *NeuroImage*, Volume 240. <https://doi.org/10.1016/j.neuroimage.2021.118407>.
- 750 Baker, A. P., Brookes, M. J., Rezek, I. A., Smith, S. M., Behrens, T., Smith, P. J. P., & Woolrich, M. (2014), *Fast transient networks in spontaneous human brain activity*. *eLife*, 3, e01867. <https://doi.org/10.7554/eLife.01867>.
- 755 Baldassano, C., Hasson, U., Norman, K. A. (2018), *Representation of Real-World Event Schemas during Narrative Perception*. *Journal of Neuroscience*, 38 (45) 9689-9699. <https://doi.org/10.1523/JNEUROSCI.0251-18.2018>.
- 760 Brookes, M.J., Woolrich, M.W., Barnes, G.R., (2012), *Measuring functional connectivity in MEG: A multivariate approach insensitive to linear source leakage*. *NeuroImage*, Volume 63, Issue 2, Pages 910-920. <https://doi.org/10.1016/j.neuroimage.2012.03.048>.
- 765 Buzsáki, G. and Draguhn, A. (2004), *Neuronal Oscillations in Cortical Networks*. *Science*, Vol 304, Issue 5679. pp. 1926-1929. [DOI: 10.1126/science.1099745](https://doi.org/10.1126/science.1099745).
- 770 Donoghue, T., Haller, M., Peterson, E.J. et al. (2020). *Parameterizing neural power spectra into periodic and aperiodic components*. *Nat Neurosci* **23**, 1655–1665. <https://doi.org/10.1038/s41593-020-00744-x>
- 775 Donoghue, T., Schaworonkow, N., & Voytek, B. (2022). *Methodological considerations for studying neural oscillations*. *European Journal of Neuroscience*, 55( 11-12), 3502– 3527. <https://doi.org/10.1111/ejn.15361>
- 780 Haynes, JD., Rees, G. (2006), *Decoding mental states from brain activity in humans*. *Nat Rev Neurosci* **7**, 523–534. <https://doi.org/10.1038/nrn1931>.
- 785 Herrmann, C. S., and Knight, R. T. (2001), *Mechanisms of human attention: event-related potentials and oscillations*. *Neurosci. Biobehav. Rev.* 25, 465–476. doi: 10.1016/S0149-7634(01)00027-6.
- 790 Higgins, C., Liu, Y., Vidaurre, D., Kurth-Nelson, Z., Dolan, R., Behrens, T., Woolrich, M. W. (2021), *Replay bursts in humans coincide with activation of the default mode and parietal alpha networks*. *Neuron*, 109 (5), pp. 882-893. <https://doi.org/10.1016/j.neuron.2020.12.007>.
- 795 Hirschmann, J., Baillet, S., Woolrich, M., Schnitzler, A., Vidaurre, D. and Florin, E. (2020), *Spontaneous network activity < 35 Hz accounts for variability in stimulus-induced gamma responses*. *NeuroImage*, Volume 207. <https://doi.org/10.1016/j.neuroimage.2019.116374>.
- 800 Huang, N.E., Wu, Z., Long, S.R., Arnold, K.C., Chen, X. and Blank, K., (2009), *On Instantaneous Frequency*. *Advances in Adaptive Data Analysis*, Vol. 01, No. 02, pp. 177-229. <https://doi.org/10.1142/S1793536909000096>.
- 805 Hyvärinen, A.; Oja, E. (2000), *Independent Component Analysis: Algorithms and Application*, *Neural Networks*, 13(4-5):411-430.
- 810 Karapanagiotidis, T., Vidaurre, D., Quinn, A.J. et al. (2020), *The psychological correlates of distinct neural states occurring during wakeful rest*. *Sci Rep* 10, 21121. <https://doi.org/10.1038/s41598-020-77336-z>.

- 795 Khawaldeh, S., Tinkhauser, G., Torrecillos, F. et al. (2022), Balance between competing spectral states in subthalamic nucleus is linked to motor impairment in Parkinson's disease. *Brain*, Volume 145, Issue 1, Pages 237–250. <https://doi.org/10.1093/brain/awab264>.
- 800 King, J.-R., and Dehaene, S. (2014), *Characterizing the dynamics of mental representations: the temporal generalization method*. Trends in Cognitive Sciences, Volume 18, Issue 4, Pages 203-210. <https://doi.org/10.1016/j.tics.2014.01.002>.
- Kotchoubey, B. (2005), *Event-related potential measures of consciousness: two equations with three unknowns*. *Prog. Brain Res.* 150, 427–444. doi: 10.1016/S0079-6123(05)50030-X.
- 805 O'Neill, G.C., Bauer, M., Woolrich, M.W., Morris, P.G., Barnes, G.R., Brookes, M.J. (2015), Dynamic recruitment of resting state sub-networks. *Neuroimage*, 115, pp. 85-95. <https://doi.org/10.1016/j.neuroimage.2015.04.030>
- 810 Picton, T. W., Bentin, S., Berg, P., Donchin, E., Hillyard, S. A., Johnson, R., et al. (2000), *Guidelines for using human event-related potentials to study cognition: recording standards and publication criteria*. *Psychophysiology* 37, 127–152. doi: 10.1111/1469-8986.3720127.
- 815 Quiñan Quiroga, R., Panzeri, S. (2009), *Extracting information from neuronal populations: information theory and decoding approaches*. *Nat Rev Neurosci* 10, 173–185. <https://doi.org/10.1038/nrn2578>.
- 820 Quinn, A.J., van Ede, F., Brookes, M.J. et al. (2019), *Unpacking Transient Event Dynamics in Electrophysiological Power Spectra*. *Brain Topogr* 32, 1020–1034. <https://doi.org/10.1007/s10548-019-00745-5>.
- Rabiner LR. (1989), *A tutorial on hidden Markov models and selected applications in speech recognition*. *Proc IEEE.*; 77(2):257–286.
- 825 Shappell, H., Caffo, B. S., Pekar, J. J., Lindquist, M. A. (2019), *Improved state change estimation in dynamic functional connectivity using hidden semi-Markov models*. *Neuroimage*, 191 pp. 243-257, [10.1016/j.neuroimage.2019.02.013](https://doi.org/10.1016/j.neuroimage.2019.02.013).
- 830 Sharma, A., Vidaurre, D., Vesper, J., Schnitzler, A., Florin, E. (2021). Differential dopaminergic modulation of spontaneous cortico–subthalamic activity in Parkinson's disease. *eLife* 10:e66057. <https://doi.org/10.7554/eLife.66057>.
- 835 Stevner, A.B.A., Vidaurre, D., Cabral, J. et al. (2019), *Discovery of key whole-brain transitions and dynamics during human wakefulness and non-REM sleep*. *Nat Commun* 10, 1035. <https://doi.org/10.1038/s41467-019-08934-3>.
- Vidaurre, D., Quinn, A.J., Baker, A.P., Dupret, D., Tejero-Cantero, A., Woolrich, M.W. (2016), *Spectrally resolved fast transient brain states in electrophysiological data*, *NeuroImage*, vol. 126, pp. 81-95. doi:10.1016/j.neuroimage.2015.11.047.
- 840 Vidaurre, D., Smith, S. M., Woolrich, M. W. (2017), *Brain network dynamics are hierarchically organized in time*. *PNAS*, 114 (48). <https://doi.org/10.1073/pnas.1705120114>.
- 845 Vidaurre, D., Hunt, L.T., Quinn, A.J. et al. (2018), *Spontaneous cortical activity transiently organises into frequency specific phase-coupling networks*. *Nat Commun* 9, 2987. <https://doi.org/10.1038/s41467-018-05316-z>.
- Vidaurre, D., Myers, N. E., Stokes, M., Nobre, A.C., Woolrich, M. W. (2019), *Temporally Unconstrained Decoding Reveals Consistent but Time-Varying Stages of Stimulus Processing*. *Cerebral Cortex*, Volume 29, Issue 2, Pages 863–874, <https://doi.org/10.1093/cercor/bhy290>

850

## FIGURES LIST

### Figure 1: Analysis workflow

Scheme of the workflow, including data, analysis type and goals of each block.

855

### Figure 2: Sensitivity analysis on the observation models

**a.** Example of signals used (stationary sinusoids), each defined by frequency, amplitude and noise variance. **b.** The plots show how the AR (left) and the TDE (right) models can tell apart two signals that differ only in frequency by an amount of  $\Delta_f$  Hz (test frequency minus training frequency), for different values of their amplitude and of their noise content. The measure used is the logarithm of the likelihood ratio between train and test signal (given a fixed test signal and models trained on many training signals). Each solid line of the plot represents analyses for noise variance equal to 0.5, and each dotted line corresponds to noise variance equal to 1.0. By manipulating amplitude and noise variance, the plots show how the models perform for different signal to noise ratio (SNR) values. Here, AR order  $P=3$ , and TDE lags  $L=21$ , in steps of  $S=1$ ; signal length  $T=10$  seconds (25000 data points)

860

**c.** AR and TDE sensitivity to amplitude, expressed as  $\Delta_a$  for the AR model (training amplitude minus test amplitude) and as training amplitude in proportion to the target test amplitude (denoted as *train/test*) for the TDE model, for different values of frequency and of noise variance. Order, lags and signal length set as in **b.**

865

### Figure 3: HMM experiments on one-channel non-stationary data

**a.** Example of signal varying in frequency (instantaneous frequency shown in the middle panel) and amplitude (instantaneous amplitude in the bottom panel). **b.** Example of the probabilistic state time courses and state power spectra of HMM-MAR and HMM-TDE applied to the signal in **a.** Here, transition probability matrix prior  $\delta = 10k$ , HMM-MAR order  $P=3$ , HMM-TDE lags  $L=15$  (in steps of  $S=3$ ). **c.** Cross validated explained variance of the HMM states predicting the ground truth frequency of non-stationary signals (like in **a.**), for 20 repetitions of the experiment, for different values of the average state switching rate, manipulated via  $\delta$  (order and lags set as in **b.**). **d.** Similarly to **a.**: example of a synthetic signal varying mostly in amplitude. **e.** Example of probabilistic state time courses and state power spectra of HMM-MAR and HMM-TDE applied to the signal in **d.** Here,  $\delta = 10k$ ,  $P=3$ ,  $L = 15$ ,  $S=3$ . **f.** Cross validated explained variance of the HMM states predicting the ground truth amplitude of the signals as a function of the average state switching rate (varying  $\delta$ , order and lags set as in **e.**), for 20 repetitions of the experiment.

870

875

880

### Figure 4: HMM experiments on two-channel data with periodic coherence

**a.** Example of the synthetic signals; instantaneous frequency is shown in the middle panel, and instantaneous correlation in the bottom panel. **b.** On the left, examples of the state time courses of HMM-MAR (top panel) and HMM-TDE (bottom panel) applied to the signal in **a.**; shown also the corresponding state power spectra (middle) and coherence (right). Here,  $\delta = 10k$ , HMM-MAR order  $P=3$ , and the HMM-TDE lags  $L=15$ , with  $S=3$ . **c.** Cross validated explained variance (CVEV) of the HMM states predicting the ground truth instantaneous frequency of the channels (average explained variance across channels, left) and channel correlation (right) for 10 repetitions of the experiment and for different values of the state switching rate, manipulated through  $\delta$ . Order and lags set as in **b.**

885

890

### Figure 5: Analysis on LFP data

**a.** LFP data, with two LFP channels (chosen such that their activity was not very correlated) from the hippocampus of a mouse during resting state, downsampled to 250 Hz, and the spectral content of the two channels. **b.** Example of HMM-MAR state time courses, as well as the state power spectra and the state coherence. **c.** Similar to **b.**, for HMM-TDE. The models are trained on 30 mins of data with three states (here, HMM-MAR order  $P=5$ , HMM-TDE, lags  $L=15$ ,  $S=3$ ,  $\delta=100k$ ).

895

### Figure 6: Analysis on MEG data

**a.** The data for this analysis are 2 MEG channels from the motor cortex of 8 (human) subjects who performed a simple finger tapping task. Data were downsampled to 200 Hz and band-filtered between 1 and 48 Hz. The spectral content of the two channels is also shown. **b.** Example of HMM-MAR state time courses, around a button press, marked by a black vertical line (left); the corresponding state power spectra (middle); and the probability of states around the button press (response-evoked state probability, rightmost panel). **c.** Same as in **b.**, for the HMM-TDE model. The models are trained on 20 mins of recordings with three states. For the HMM-MAR we used order  $P=3$ , and for the HMM-TDE we used  $L=1$ , with  $S=1$ ;  $\delta=100000$  in both cases.

900

905